Water Research X 24 (2024) 100245

Contents lists available at ScienceDirect

Water Research X

journal homepage: www.sciencedirect.com/journal/water-research-x

Towards stable and efficient nitrogen removal in wastewater treatment processes via an adaptive neural network based sliding mode controller

Yiqi Liu [*,a,b], Jing Zhang [a,b], Zhuyi Qiu [a,b], Yigang Zhang [a,b], Guangping Yu [c], Hongtao Ye [d], Zefan Cai [e]

[a] Key Laboratory of Autonomous Systems and Networked Control, Ministry of Education, School of Automation Science & Engineering, South China University of Technology, Guangzhou, 510640, China
[b] Guangdong Engineering Technology Research Center of Unmanned Aerial Vehicle Systems, School of Automation Science & Engineering, South China University of Technology, Guangzhou, 510640, China
[c] Guangzhou Institute of Industrial Intelligence, Guangzhou, 511458, China
[d] School of Automation, Guangxi University of Science and Technology, Liuzhou 545036, China
[e] College of Intelligent Manufacture, ShunDe Polytechnic, Foshan Guangdong 528333, China

ARTICLE INFO

Keywords:
Wastewater treatment processes
Sliding mode control
BSM2
Adaptive neural network

ABSTRACT

Advanced controllers often offer an innovative solution to proper quality control in wastewater treatment processes (WWTPs). However, nonlinearity and uncertain disturbances usually make the conventional control strategies inadequate or impossible for the stable operations of WWTPs. To guarantee the stability of ammonia nitrogen concentration (S_{NH}) control in WWTPs, a direct adaptive neural networks-based sliding mode control (ANNSMC) strategy has been proposed in this article. A sliding mode controller is designed and implemented with the help of an adaptive Neural Network (ANN), named Radial Basis Function Neural Network (RBFNN), which can approach the desired control law accurately. Also, the stability of a system installed with the ANNSMC is analyzed by using the Lyapunov theorem, which ensures system robustness and adaptability. Additionally, to deal with high energy consumption and low treatment efficiency problems in the wastewater denitrification processes, this paper proposes a dual-loop denitrification control strategy and validates it in the Benchmark Simulation Model No.2 (BSM2) platform. The strategy can strengthen the denitrification efficiency by collaborating the S_{NH} with nitrate nitrogen (S_{NO}) concentration in the WWTPs properly. The experimental results demonstrate that the proposed strategy can obtain remarkable stability and robustness, reducing energy consumption effectively compared with other standard and advanced control strategies.

1. Introduction

With the ever-increasing requirements of more stringent regulations, more energy saving, less greenhouse gas emissions and more stable and efficient operations of WWTPs have become a hot research area Ching et al. (2021); Li et al. (2024); Liu et al. (2023). In WWTPs, nitrogen removals can have a serious negative impact on the environment, and even result in the eutrophication problems in water bodies if not well controlled. Therefore, efficient nitrogen removal in wastewater, especially ammonium, nitrate, nitrite and total nitrogen (TN), in the effluent, is of great importance in WWTPs Zhang et al. (2023).

Activated sludge processes (ASPs) are widely recognized as the predominant wastewater treatment methodologies in practice, which adopt nitrification-denitrification reactions to remove nitrogen Baeten et al. (2019); Liu et al. (2020). Proportional Integral Ierivative (PID) controller is a simple but powerful way to control nitrogen removal by manipulating the dissolved oxygen (DO) Iratni and Chang (2019); Tzoneva (2007). In these control strategies, the P, I, D parameters are optimized by trials and errors offline and are fixed for online usage, However, dynamic behaviors and disturbances usually frustrate standard PID controllers with fixed parameters. With the wave of artificial intelligence and digitalization, new PID control methods have been proposed to ensure P, I, D can be manipulated adaptively Harja et al. (2016); Vilanova et al. (2009); Wahab et al. (2007); Ye et al. (2013). In these methods, Vilanova et al. developed a decentralized control strategy as well as a PID adjusting method for multi-loop control for ASP

* Corresponding author.
E-mail address: aulyq@scut.edu.cn (Y. Liu).

https://doi.org/10.1016/j.wroa.2024.100245
Received 13 March 2024; Received in revised form 21 June 2024; Accepted 25 July 2024
Available online 30 July 2024

Vilanova et al. (2009). Ye et al. employed fuzzy sets to find the optimal PID parameters,then bettering DO control performance Ye et al. (2013). However, most of these methods regard the biochemical reaction as a linear process, in which the biological parameter values are assumed to be known in advance, which is obviously inconsistent with the strong nonlinear and strongly coupled characteristics of actual wastewater treatment. With the wave of Industry 4.0 and artificial intelligence (AI), researchers have proposed a large amount of intelligent control strategies to deal with these problems. Piotrowski et al. developed a model predictive control (MPC) algorithm and used it to control DO in Sequencing Batch Reactor (SBR) Piotrowski et al. (2021). The algorithm can determine the control law of the output by predicting the future value of DO. The simulation results indicated that MPC can meet the control requirements while reducing energy consumption. Monteiro et al. designed an optimal control algorithm by trading off the requirements of DO and effluent qualities Monteiro et al. (2022). In this methodology, they turned the optimal problem into a nonlinear optimization problem through discretization, thus simplifying the optimization and reducing energy consumption. In Han et al. (2020), a synergistic fuzzy neural controller was designed, which was adapted to the time-varying characteristics of wastewater treatment via coordinating global parameters to optimize the output control law, and the resulted findings suggested that the proposed method can achieve better control performance with less computational consumption. Due to the large computational burden of traditional networks, Cao et al. put forward an adaptive control method with the help of an online sequential extreme learning machine, which can take advantage of fast online training. The proposed method showed good control characteristics in simulation experiments Cao and Yang (2020). In addition to this, many other methods have shown good control performance in the wastewater treatment process Boruah and Roy (2019); Chen et al. (2021); Han et al. (2021). However, these methods usually require complex and intensive online optimization calculations, resulting in heavy controller structure and unacceptable computational load. In addition, since WWTPs usually exposed to uncertainties, such as unknown weather conditions, it is difficult to guarantee robust operations with the conventional control strategies Boiocchi et al. (2016); Du et al. (2022). To overcome these constraints and to facilitate stable operations of wastewater treatment systems, advanced control strategies have received more and more attention Li et al. (2022).

Sliding mode control (SMC) is a commonly used nonlinear control method, through the introduction of sliding surface and control law to induce the system state to slide along the designated surface, in such a way that the desired control objectives can be achieved. SMC has strong robustness and can depress the system parameter changes, external disturbances and modeling errors. Therefore, in recent years, SMC has received extensive attention from academic and industrial communities. MuȘoz et al. proposed a SMC to control the concentration of DO in the denitrification process in SBR, and the experimental results showed that satisfactory control performance of SMC can be achieved Munoz et al. (2009). In Riaz et al. (2023), Riaz et al. proposed a SMC that can be predefined in time and applied to address the position control challenges in permanent magnet linear motors, and the simulation results demonstrate the method's ability to achieve convergence within the designated timeframe. Fujio et al. defined a PID sliding mode surface by combining SMC with PID and used it for the dynamic control of a soft robot, and the results exhibit the potential to enhance the precision of the soft robot and can reduce the amplitude well Fujio et al. (2016). However, all of these sliding mode controllers require accurate system model, which could be difficult or even impossible for complex systems. Moreover, the design of SMC usually requires the selection of appropriate sliding mode surfaces and SMC laws, which depends heavily on a certain amount of experience and expertise. Since WWTPs are a highly complex system and is difficult to determine an accurate mechanistic model, the research about applications of SMC to a WWTP system is still limited and falls in the early stage.

Inspired by the above analysis, this paper proposes ANNSMC to promote the nitrogen removal efficiency with less energy consumption in WWTPs. Artificial neural networks can provide a powerful tool to deal with nonlinear issues for WWTPs. By learning the relationship between inputs and outputs, Adaptive neural networks (ANNs) are able to automatically adjust their weights and parameters to map the inputs optimally and output the corresponding prediction or decision results correctly DeVore et al. (2021); Pozevalkin et al. (2019). In this light, ANN can work together with SMC and a new controller is designed and a new control structure can be formulated. The main contributions of this study are outlined as follows:

(1) A new set of controllers, called ANNSMC, was designed and used in a cascade control strategy to control ammonia concentration by regulating the dissolved oxygen in the proper location of WWTPs. This method employs an adaptive neural network to approach the model nonlinearity and uncertainties, and effectively bettering control performance.
(2) Considering the stability and fast convergence within the entire control system, the adaptive rate of RBFNN is validated and has been proven by Lyapunov method. The RBFNN can facilitate weight optimization adaptively, thus achieving more accurate control.
(3) To better treatment efficiency with lower energy consumption in the denitrification process, a dual-loop denitrification control system is proposed. This system can ensure better TN quality in the effluent by considering both behaviors of nitrification and denitrification.

The remaining sections of this paper are organized as follows. Section II, simulation experiments on the BSM2 platform and discussion. Section III, gives a conclusion. Section IV,provides a description of the materials and methods, and gives a stability proof.

Notations: In the paper, $\|\cdot\|$ represents the Euclidean norm of vectors and the induced norm of matrices.$|\cdot|$ represents the absolute value. $\widehat{V}$ and $\widetilde{V}$ represent the estimate of the corresponding parameter V and the error in the estimate, respectively. $[\cdot]^T$ denotes transpose.$\dot{v}$ and $\ddot{v}$ represent first-order and second-order derivatives, respectively.

2. Results and discussion

2.1. Scenario definition

In this paper, the proposed control structure shown in Fig. 1 is adopted. All experiments in this paper were conducted and validated depending on the BSM2 platform in the MATLAB environment.

2.1.1. Experiment of ANNSMC performance

To demonstrate the comprehensiveness of the proposed controller, experiments were carried out in this paper under different influent conditions and setpoints, namely: *Case 1*: static influent conditions with a constant setpoint (ref=1). *Case 2*: static influent conditions with changing setpoints. *Case 3*: dynamic influent conditions with tracking of a constant setpoint.

To better verify the performance of ANNSMC, PID and Active Disturbance Rejection Controller (ADRC) are also introduced for comparison. We chose three performance metrics, namely, Integral Absolute Error (*IAE*), Integrated Squared Error (*ISE*) and Integrated Time Absolute Error (*ITAE*), to comprehensively evaluate the control system from multiple perspectives. The formula is shown below:

$$IAE = \int_0^\infty |e(t)|dt \tag{1}$$

$$ISE = \int_0^\infty e^2(t)dt \tag{2}$$

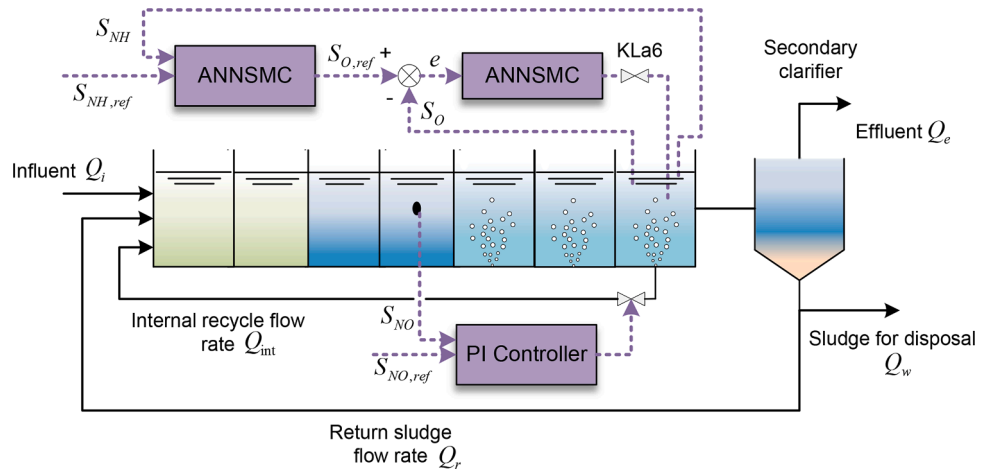

Fig. 1. The proposed dual-loop denitrification control strategy

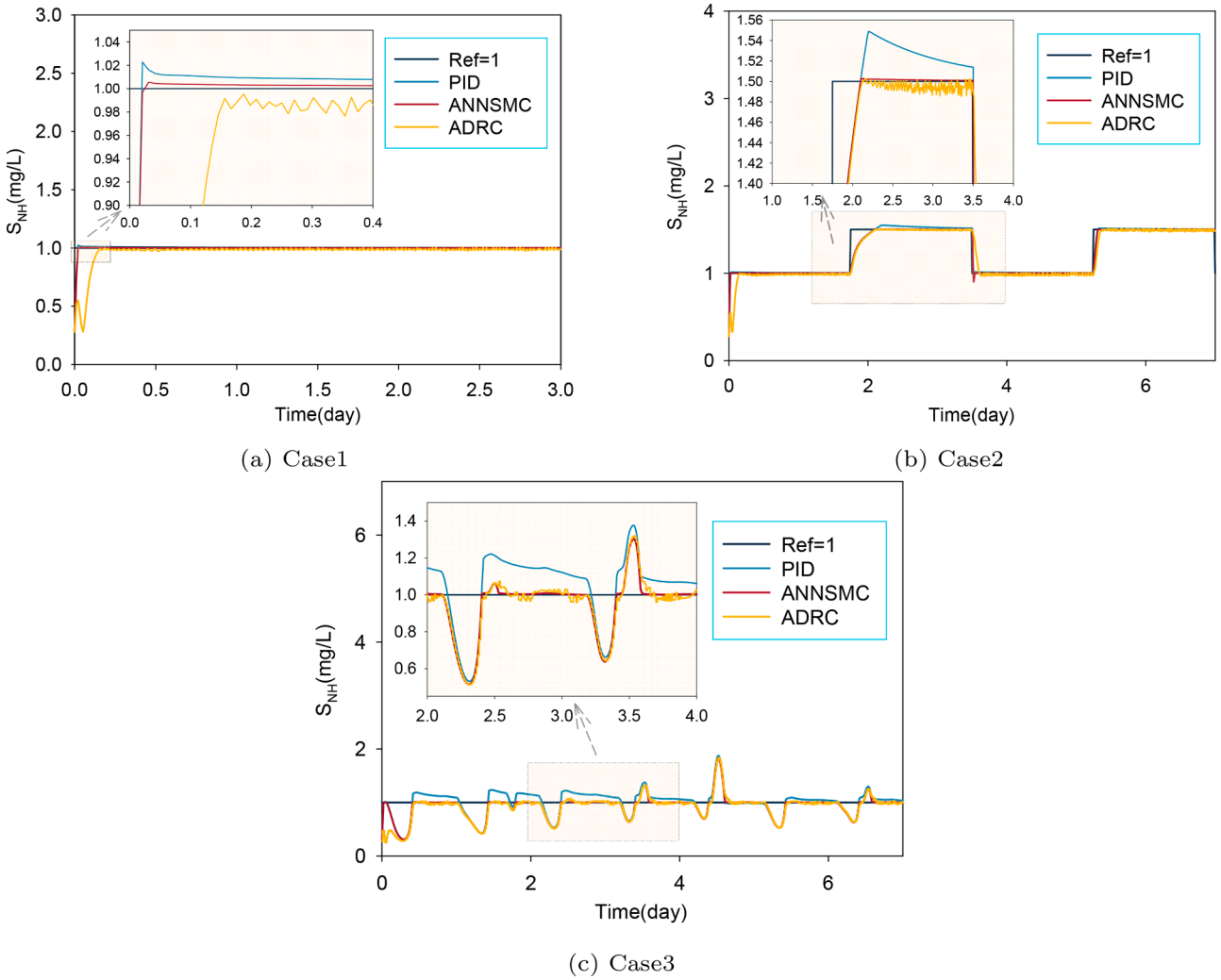

Fig. 2. Control tracking results of S_{NH} in different cases

$$ITAE = \int_0^{\infty} t|e(t)|dt \tag{3}$$

From the formula, it can be seen that *IAE* can respond to the deviations properly in the control process; *ISE* can highlight how large deviations affect the control performance; and *ITAE* can indicate the error evolution over time variations in the control process.

To achieve better controller, this paper uses genetic algorithm (GA) to optimize the parameters of the controller. By trading off the control stability, accuracy and adaptability of the system, the fitness function of the GA is chosen as follows:

$$F = \int_0^{\infty} \delta_1 t|e(t)|dt + \delta_2 M_p + \delta_3 t_s \tag{4}$$

Where, M_p denotes the degree of overshooting, t_s is the settling time, $\delta_1, \delta_2, \delta_3$ represent the weights for different components.

After global optimization of the controller parameters by GA, the main parameters of ANNSMC are designed as follows: the sliding mode surface error weights parameter $\lambda = 5.57$; the RBFNN Gaussian basis function neuron width $b = 19.1501$. The neuron center point c is:

$$c = 19.1501 * \begin{bmatrix} -3 & -2.5 & -2 & -1.5 & -1 & -0.5 & 0 & 0.5 & 1 & 1.5 & 2 & 2.5 & 3 \\ -3 & -2.5 & -2 & -1.5 & -1 & -0.5 & 0 & 0.5 & 1 & 1.5 & 2 & 2.5 & 3 \\ -3 & -2.5 & -2 & -1.5 & -1 & -0.5 & 0 & 0.5 & 1 & 1.5 & 2 & 2.5 & 3 \\ -3 & -2.5 & -2 & -1.5 & -1 & -0.5 & 0 & 0.5 & 1 & 1.5 & 2 & 2.5 & 3 \\ -3 & -2.5 & -2 & -1.5 & -1 & -0.5 & 0 & 0.5 & 1 & 1.5 & 2 & 2.5 & 3 \end{bmatrix}$$

The other parameters are: $\sigma = 0.005$, $k = 0.25$, $\Gamma = 225 * eye(13)$($eye(\cdot)$ denotes the unit matrix).

2.1.2. Experiment design of the dual-loop control strategy

By analysis, it is obvious that ammonia nitrogen is correlated with nitrate nitrogen fairly. Ammonia nitrogen undergoes nitrification reactions and is converted into nitrate nitrogen in the nitrification process, while nitrate nitrogen can be transformed into nitrogen gas through denitrification process. Consequently, setting up a proper setpoint for S_{NH} has an influential impact on the S_{NO} control in the reactors. Therefore, we tested the tracking of nitrate nitrogen under different S_{NH} setting points by taking into account the influent conditions and pattern analysis.

When designing the dual-loop control strategy, the first control loop is controlled by ANNSMC. Due to the internal recycle flow rate of 61944 m^3/d in BSM2, it is challenging to effectively manipulate the control law of ANNSMC within such a significant delay and multivariable interplay. To simplify the control challenge, the second control (inner) loop uses a PID controller to maintain the nitrate nitrogen concentration at a predetermined level. The parameters of ANNSMC is set up as in Section 2.1.1. The parameters of the PID controller are set as follows after GA rectification: the proportional coefficient $K_p = 155$, integral coefficient $K_i = 0.02$, differential coefficient $K_d = 1.2$.

The main purpose of a WWTP to control the S_{NH}, S_{NO}, TN in the effluent and aeration energy (AE) consumption overall. The AE consumption of the system can be calculated from the following formula:

$$AE = \frac{S_{O,15}^{sat}}{t_{obs} \cdot 1.8 \cdot 1000} \int_{t_{start}}^{t_{end}} \sum_{i=1}^{i=5} V_i \cdot K_L a_{i,15}(t) dt \tag{5}$$

Where, t_{obs} is the evaluation period (day), V_i represents the volume of reaction unit i (m^3). $K_L a_{i,15}$ denotes the oxygen mass transfer coefficient in unit i, and $S_{O,15}^{sat}$ represents the DO saturation concentration at (both of them are at 15.

In this article, two additional control schemes are chosen for comparison, respectively: *S1*: BSM2 default control scheme; *S2*:the proposed ANNSMC based cascade control in the single loop; S3: The proposed dual-loop control scheme.

2.2. Performance comparisons

Fig. 2 gives the tracking curves of the controller for different setpoints as well as influent conditions. To provide more details about the controller's performance, the IAE, ISE and ITAE with respect to the controllers under different conditions are tabulated in Table 1.

As can be seen in Fig. 2a, given a constant signal, all three controllers can meet the control requirements, of which ADRC exhibits slight oscillations after reaching stability. However, when given signal changes to the changing signal as shown in Fig. 2b, all three controllers show a slower response speed at the first rising edge of the square wave signal, but can achieve better performance for the falling side. Among them, PID exhibits obvious overshooting behaviors, and ADRC also has more obvious oscillations. The proposed ANNSMC, on the other hand, can outperform the other two controllers in both the settling time and the convergence speed. In terms of the performance metrics under static influent conditions, it is clear that both IAE and ITAE of ANNSMC are almost twice small than PID controller, and lower than ADRC significantly. This demonstrates that, under the static influent case, ANNSMC exhibits the best performance in terms of stability and robustness. That is because the adaptive RBFNN can better approach the system dynamics model by constantly updating the network weight and thus outputting a proper control law, and the combination of adaptive capabilities allows the controller to control the variables at a faster rate and with higher accuracy, therefore resulting in better performance.

For the dynamic influent condition, it can be seen from Fig. 2c that, although all three controllers have a specified degree of overshoot and undershoot, ANNSMC and ADRC demonstrate better control performance compared to the PID. It is also obvious from the performance indicators in Table 1 that the ANNSMC and ADRC have similar values, both of which are significantly lower than those of the PID controller. This indicates that ANNSMC and ADRC have stronger disturbance rejection capabilities compared to the PID. Additionally, as can seen in Fig. 2c there is an obvious oscillation phenomenon when ADRC converges, while ANNSMC is smoother and has no obvious oscillations. That is because the control rate of ANNSMC is derived from the Lyapunov function, which ensures the semi-global boundedness of the controlled system, thus improving system robustness and making it better resistant to disturbances.

In summary, the ANNSMC designed in this paper has good tracking performance and exhibits acceptable stability and robustness.

Fig. 3 shows the control performance of nitrate nitrogen under different setpoints of ammonia nitrogen concentration.

As can be seen from the curve profiles in Fig. 3, when the S_{NH} is set to 0.1 mg/L, a good tracking performance can be achieved for S_{NO}. Therefore, this paper selects 0.1 mg/L as the S_{NH} setting value by cross validations, then to construct the dual-loop nitrogen removal control system. Table 2 shows the average value of nitrogen-related variables in the effluent of biochemical reactor, along with the energy consumption for each scheme.

As shown in the Table 2, it is evident that, compared to the default control scheme, the proposed dual-loop denitrification control structure in this paper achieved a reduction in S_{NO} by 15.5%. Although the ammonia nitrogen content showed a slight increase, TN in the effluent decreased by 8.2%. Additionally, the average AE consumption has also been reduced. However, simply controlling DO not only fails to reduce the effluent TN content but also increases energy consumption. This is

Table 1
Comprehensive performance index of the controller for different input cases

Controller	Case1			Case2			Case3		
	IAE	ISE	ITAE	IAE	ISE	ITAE	IAE	ISE	ITAE
PID	0.0213	0.003	0.0285	0.1462	0.0229	0.4064	1.1949	0.3917	3.4402
ADRC	0.1088	0.0102	0.3088	0.1278	0.0133	0.3229	0.7972	0.3313	2.2925
ANNSMC	0.0113	0.003	0.0115	0.0824	0.0216	0.2106	0.8881	0.3567	2.5364

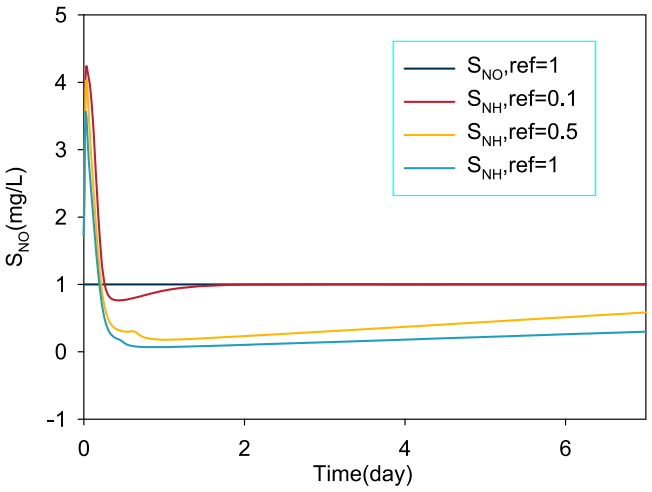

Fig. 3. Tracking results under dynamic influent conditions

Table 2
Average total nitrogen and energy consumption in Bioreactor Effluent

Control method	S_{NO}(mg/L)l	S_{NH}(mg/L)	TN(mg/L)	AE(kWh/d)
S1	8.0885	1.3448	11.9746	6630.75
S2	13.2426	3.0087	18.8102	6730.9
This paper	6.8337	1.6156	10.9948	6586.89

because the aeration process requires energy input to generate oxygen and deliver it to the biological treatment unit. Consequently, when only controlling the DO level, an increase in aeration rate is necessary to meet the requirements, resulting in an escalation of energy consumption. The dual-loop structure designed in this paper can accurately control the S_{NH} and S_{NO} in the effluent and avoid the ammonia nitrogen or nitrate nitrogen out of the required range. When S_{NH} is controlled and maintained at a desired level, the oxygen demand for nitrification reaction can be reduced accordingly, thereby reducing unnecessary aeration and lowering the corresponding energy consumption. Besides, via controlling the internal recycle flow rate during denitrification, the denitrification efficiency can be optimized, thereby making aeration energy consumption even lower. Therefore, the dual-loop control strategy proposed in this article can achieve better denitrification effects with lower AE consumption.

3. Conclusion

In this study, a novel adaptive controller, ANNSMC, was designed and successfully applied to the precise control of the SNH in WWTPs. To ensure lower TN in the effluent with lower AE consumption, a dual-loop denitrification control structure is also proposed. The experimental results show that the ANNSMC has better control performance than the traditional PID control, with better stability and faster convergence speed Furthermore, the experiment results demonstrate that the dual-loop denitrification control strategy can achieve excellent performance in controlling TN in the effluent with less energy consumption. Compared with the scenario without a controller, the TN in the effluent is reduced by 8.2%, and the average AE consumption is reduced by 43.86kWh/d. The current work only discusses nitrogen removal in WWTPs. This paper not only proposes a novel adaptive control method, but also shows better control performance and more energy-saving effects in practical application, providing a new solution for the intelligent operation of wastewater treatment plants. Future work will further focus on the simultaneous removal of total phosphorus (TP) together with TN and consider the control of more quality indexes in the effluent, to realize the optimization of wastewater treatment globally.

4. Materials and methods

4.1. Wastewater treatment system for validation

To better compare different control strategies, BSM2 was first proposed and supported by the European Union Organization for Scientific and Technological Cooperation (COST) 624 Program project meeting Jeppsson et al. (2007). As shown in Fig. 4, this is a schematic plant model of WWTP, including a primary sedimentation tank, activated sludge reactor, secondary sedimentation tank, anaerobic digester, thickener and dewatering unit. This platform can represent most general WWTP with the biological activated sludge method used for nitrogen removal. The activated sludge reactors consist of two anoxic units, two anaerobic units, and three aerobic units. In WWTPs, organic matter was reduced into ammonia nitrogen by ammonification in the anoxic environment. Subsequently, nitrification reactions occur under aerobic conditions to convert the ammonia nitrogen into nitrate and nitrite. Then the nitrate nitrogen has been reintroduced to the anoxic units for denitrification through the internal recycle flow, resulting in the conversion of nitrate nitrogen into nitrogen gas and its subsequent release.

From the above analysis, it can be seen that there is a complex interconversion relationship between ammonia nitrogen and nitrate nitrogen, and it is difficult for a single control loop to maintain the balance between them. Moreover, the internal and external cycles of wastewater make wastewater treatment characterized by nonlinearity and multivariate nexus. Therefore, this paper presents a dual-loop control system in Fig. 4 to control the effluent quality properly with less energy consumption. The proposed structure can independently regulate ammonia nitrogen and nitrate nitrogen to a desired level, which can optimize overall performance efficiently. In the reaction tank, the concentrations of DO, S_{NH} and S_{NO} interact with each other. If there is too much DO, S_{NH} decreases and S_{NO} increases, and conversely, too little DO increases S_{NH} and decreases S_{NO}. Therefore, it is important to reasonably set the setting value of DO concentration. The first control loop in this paper uses the ammonia in the aerobic zone to determine the optimum DO set point. The second control loop regulates the S_{NO} by controlling the internal return flow.

Typical patterns can be observed in simulated wastewater treatment plants within a year as the true WWTP, such as dry weather, rainy days, stormy days, etc., which fully takes into account seasonal variations, diurnal variations, holiday variations, and potential factors.

4.2. Problem formulation

To maintain the concentration of a variable at a given value, it is necessary to design a suitable controller that can meet the control requirements. However, due to the underlying complexity of WWTPs, it is difficult to understand the nonlinear, multivariate and uncertain characteristics of WWTPs, thus this adds more difficulties in designing a proper control law Cheng et al. (2021); Han et al. (2018). In addition, time delay happens around the entire WWTP because of mixing substrate, mass transfer and biological reactions. Therefore, we considered the use of a second-order nonlinear system as a kinetic model for the activated sludge reactors. Without loss of generality, in this paper, the equivalent model of the biological activated sludge component is defined as the following nonlinear dynamic system:

$$\begin{cases} \dot{x}_1 = x_2 \\ \dot{x}_2 = f(\mathbf{x}) + g(\mathbf{x})u + d(t) \\ y = x_1 \end{cases} \tag{6}$$

Where, $\mathbf{x} = [x_1, x_2]^T \in R^2$ represents the state variable of the system. u represents the control input, and y represents the system output. $f(\mathbf{x})$ and $g(\mathbf{x})$ denote unknown nonlinear function affecting the controlled and control quantities. $d(t)$ is a bounded external disturbance signal. $0 < d$ and $|d(t)| \leqslant d$.

In practical WWTPs, owing to the $f(\mathbf{x})$ and $g(\mathbf{x})$ cannot be specifically

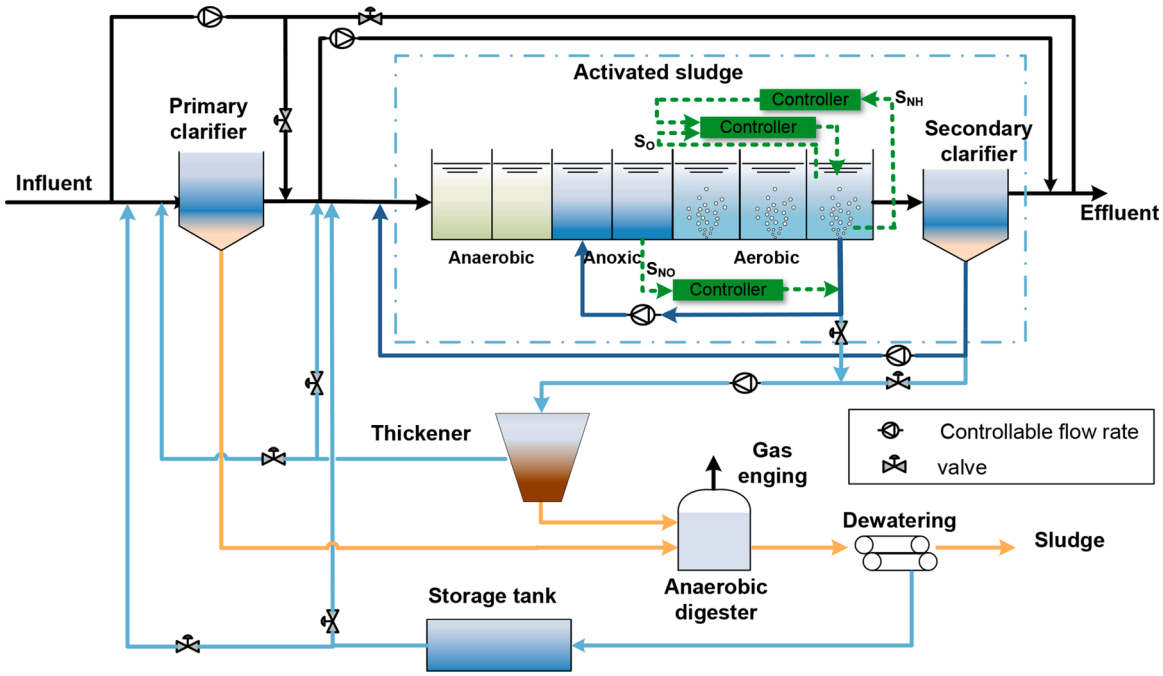

Fig. 4. Wastewater Optimization Scheme Structure

given, as well as the presence of numerous frequent disturbances in WWTP, such as influent fluctuations, weather changes, etc., the control law cannot be given or calculated directly. Therefore, due to the above reasons, we give the following control strategy based on RBFNN.

4.3. Adaptive neural network based sliding mode control (ANNSMC)

In the proposed scheme, the ANNSMC is employed to regulate the S_{NH} as well as the DO concentration, in such a way that the setting point can be tracked quickly and stationarily. Fig. 5 shows the designed control structure of ANNSMC, where the RBF model is used to approach the nonlinear relationship, which would approximate the control law and improve the controllers adaptability in WWTPs. More details about the RBF model can be seen in the Supplementary Information.

4.3.1. Desired SMC law design

In order to better satisfy the required robustness and stability of the control, we first design an ideal control law based on system characteristics

For the system shown in Eq. 6, the vectors X_d, E and the sliding mode surface s are defined as follows:

$$\begin{cases} X_d &= [y_d \quad \dot{y}_d]^T \\ E &= \mathbf{x} - X_d = [e \quad \dot{e}]^T \\ s &= [\lambda \quad 1]E = \lambda e + \dot{e} \end{cases} \tag{7}$$

Where, $\lambda \geqslant 1$, X_d is the desired trajectory vector, which is known and characterized by continuous values, y_d is the desired tracking signal, and $e = y - y_d = x_1 - y_d$ is the error, thus:

$$\begin{aligned} \dot{s} &= \lambda\dot{e} + \ddot{e} = \lambda\dot{e} + \ddot{x}_1 - \ddot{y}_d \\ &= \lambda\dot{e} + f(\mathbf{x}) + g(\mathbf{x})u - \ddot{y}_d + d(t) \\ &= f(\mathbf{x}) + g(\mathbf{x})u + v + d(t) \end{aligned} \tag{8}$$

$$v = -\ddot{y}_d + \lambda\dot{e} \tag{9}$$

For the dynamic system shown in Eq. 6, formulate the desired SMC row u^*:

$$u^* = -\frac{1}{g(\mathbf{x})}(f(\mathbf{x}) + v) - \left(\frac{1}{kg(\mathbf{x})} + \frac{1}{kg^2(\mathbf{x})} - \frac{\dot{g}(\mathbf{x})}{2g^2(\mathbf{x})}\right)s \tag{10}$$

Where, k is the design parameter and $k > 0$, k would affect the convergence speed. $\lim_{t\to\infty} \| e(t) \| = 0$ is established. The proof is given below:

Replace $u = u^*$ in Eq. 8, then:

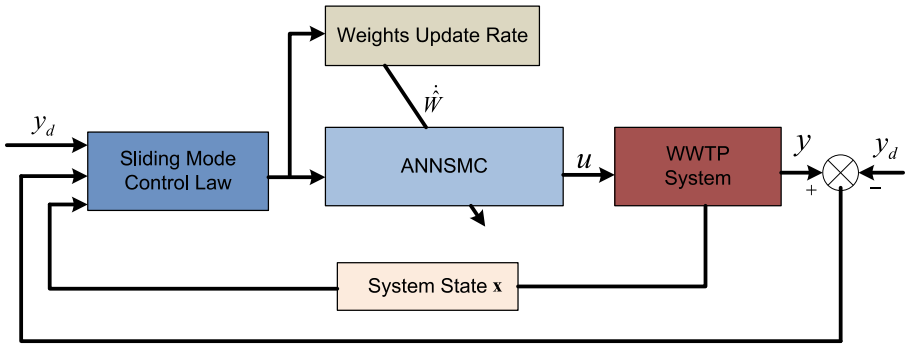

Fig. 5. ANNSMC Structure

$$\dot{s} = f(\mathbf{x}) + v + g(\mathbf{x})\left(-\frac{1}{g(\mathbf{x})}(f(\mathbf{x}) + v) - \left(\frac{1}{kg(\mathbf{x})} + \frac{1}{kg^2(\mathbf{x})} - \frac{\dot{g}(\mathbf{x})}{2g^2(\mathbf{x})}\right)s\right) = -\left(\frac{1}{k} + \frac{1}{kg(\mathbf{x})} - \frac{\dot{g}(\mathbf{x})}{2g(\mathbf{x})}\right)s \tag{11}$$

$$s\dot{s} = s\left[-\left(\frac{1}{k} + \frac{1}{kg(\mathbf{x})} - \frac{\dot{g}(\mathbf{x})}{2g(\mathbf{x})}\right)s\right] \tag{12}$$

Choose the Lyapunov function as $V = \frac{1}{2g(\mathbf{x})}s^2$, such that:

$$\begin{aligned}\dot{V} &= \frac{1}{g(\mathbf{x})}s\dot{s} - \frac{\dot{g}(\mathbf{x})}{2g^2(\mathbf{x})}s^2 \\ &= \frac{1}{g(\mathbf{x})}s\left[-\left(\frac{1}{k} + \frac{1}{kg(\mathbf{x})} - \frac{\dot{g}(\mathbf{x})}{2g(\mathbf{x})}\right)s\right] - \frac{\dot{g}(\mathbf{x})}{2g^2(\mathbf{x})}s^2 \\ &= -\left(\frac{1}{kg(\mathbf{x})} + \frac{1}{kg^2(\mathbf{x})}\right)s^2 \leqslant 0\end{aligned} \tag{13}$$

Eq. 13 indicates that the smaller the k value, the more negative the $\dot{V}$ value, From Lyapunov stability theory, we can know that $\lim_{t\to\infty} \| s \| = 0$ and $\lim_{t\to\infty} \| e(t) \| = 0$ is established, and the speed of convergence can be accelerated by choosing the appropriate parameter k.

4.3.2. ANNSMC design

In Section 4.3.1 we obtained the ideal control law for the system and proved its stability. However since the $f(\mathbf{x})$ and $g(\mathbf{x})$ are unknown, the existence of the control control law u^* in Eq. 10 is unattainable. Hence, RBFNN is used to approach the control law u^*, which compensates for the uncertainty of the system. From Eq. 10, u^* is the continuous function about $\mathbf{x}, s, k, v$, so the input $\mathbf{z}$ of the neural network can be defined as follow:

$$\mathbf{z} = \left[\mathbf{x}^T, s, \frac{s}{k}, v\right]^T \in \Omega_z \subset R^5 \tag{14}$$

$$\Omega_z = \left\{ \left(\mathbf{x}^T, s, \frac{s}{k}, v\right) | \mathbf{x} \in \Omega_x; | s = [\lambda, 1]E; | v = -\ddot{y}_d + \lambda\dot{e} \right\} \tag{15}$$

When the system state variables trajectories can be maintained within a bounded compact set Ω_z, define an ideal network weight W^*, such that the neural network output could approximate the control law u^*. Then the neural network output is:

$$u^*(\mathbf{z}) = W^{*T}H(\mathbf{z}) + \varepsilon(\mathbf{z}), \quad \forall \mathbf{z} \in \Omega_z \tag{16}$$

Where, $H(\mathbf{z})$ denotes the Gaussian basis function, $\varepsilon(\mathbf{z})$ denotes the network estimation error, $\bar{\varepsilon}$ denotes the upper limit of the approximation error, $|\varepsilon| \leqslant |\bar{\varepsilon}|$.

However, since the network weight W^* is unknown, the actual output of the controller is:

$$u = \widehat{W}^T H(\mathbf{z}) \tag{17}$$

Where, $\widehat{W}$ is the estimated network weight of the ideal weight W^*. The adaptive law can be designed as:

$$\dot{\widehat{W}} = -\Gamma(H(\mathbf{z})s + \sigma\widehat{W}) \tag{18}$$

Where, $\Gamma = \Gamma^T > 0$ represents the adaptive gain matrix. σ is the correction parameter, $\sigma > 0$.

Substituting Eq. 17 into Eq. 8 :

$$\dot{s} = f(\mathbf{x}) + v + g(\mathbf{x})\widehat{W}^T H(\mathbf{z}) + d(t) \tag{19}$$

Further substitute Eq. 16 into Eq. 19 to get:

$$\begin{aligned}\dot{s} &= f(\mathbf{x}) + v + g(\mathbf{x})\widehat{W}^T H(\mathbf{z}) - g(\mathbf{x})\left[W^{*T}H(\mathbf{z}) + \varepsilon(\mathbf{z})\right] + g(\mathbf{x})u^*(\mathbf{z}) + d(t) \\ &= f(\mathbf{x}) + v + g(\mathbf{x})\left[\widetilde{W}^T H(\mathbf{z}) - \varepsilon(\mathbf{z}) + u^*(\mathbf{z})\right] + d(t)\end{aligned} \tag{20}$$

Substituting u^*e in Eq. 10 into Eq. 20 we get:

$$\begin{aligned}&\dot{s} = g(\mathbf{x})\left[\widetilde{W}^T H(\mathbf{z}) - \varepsilon(\mathbf{z})\right] - s\left[\frac{1}{k} + \frac{1}{kg(\mathbf{x})} - \frac{\dot{g}(\mathbf{x})}{2g(\mathbf{x})}\right] + d(t) \\ &\widetilde{W} = \widehat{W} - W^*\end{aligned} \tag{21}$$

4.4. Stability analysis

In this section, the stability of the controlled system will be analyzed using the Lyapunov stability theory.

To prevent $g(\mathbf{x})$ from being included in the adaptive law $\dot{\widehat{W}}$, we choose the Lyapunov function as:

$$V = \frac{1}{2}\left(\frac{s^2}{g(\mathbf{x})} + \widetilde{W}^T\Gamma^{-1}\widetilde{W}\right) \tag{22}$$

Combining Eq. 18 and Eq. 21, we differentiate on time t to derive:

$$\begin{aligned}\dot{V} &= \frac{s\dot{s}}{g(\mathbf{x})} - \frac{\dot{g}(\mathbf{x})s^2}{2g^2(\mathbf{x})} + \widetilde{W}^T\Gamma^{-1}\dot{\widetilde{W}} = \frac{s\dot{s}}{g(\mathbf{x})} - \frac{\dot{g}(\mathbf{x})s^2}{2g^2(\mathbf{x})} + \widetilde{W}^T\Gamma^{-1}\dot{\widehat{W}} \\ &= \frac{s}{g(\mathbf{x})}\left\{g(\mathbf{x})\left[\widetilde{W}^T H(\mathbf{z}) - \varepsilon(\mathbf{z})\right] - s\left[\frac{1}{k} + \frac{1}{kg(\mathbf{x})} - \frac{\dot{g}(\mathbf{x})}{2g(\mathbf{x})}\right] + d(t)\right\} - \frac{\dot{g}(\mathbf{x})s^2}{2g^2(\mathbf{x})} \\ &\quad + \widetilde{W}^T\Gamma^{-1}\left[-\Gamma(H(\mathbf{z})s + \sigma\widehat{W})\right] \\ &= -\left(\frac{1}{kg(\mathbf{x})} + \frac{1}{kg^2(\mathbf{x})}\right)s^2 + \frac{sd(t)}{g(\mathbf{x})} - \varepsilon(\mathbf{z})s - \sigma\widetilde{W}^T\widehat{W}\end{aligned} \tag{23}$$

According to the fundamental inequality theorem ($2ab \leqslant a^2 + b^2$), the following inequality can be obtained as follows:

$$\begin{aligned}-\sigma\widetilde{W}^T\widehat{W} &= -\frac{\sigma}{2}\left[\widetilde{W}^T(\widetilde{W} + W^*) + (\widehat{W} - W^*)^T\widehat{W}\right] \\ &= -\frac{\sigma}{2}\left[\widetilde{W}^T\widetilde{W} + (\widehat{W} - W^*)^T W^* + \widehat{W}^T\widehat{W} - W^{*T}\widehat{W}\right] \\ &= -\frac{\sigma}{2}\left(\| \widetilde{W} \|^2 + \| \widehat{W} \|^2 - \| W^* \|^2\right) \\ &\leqslant -\frac{\sigma}{2}\left(\| \widetilde{W} \|^2 - \| W^* \|^2\right)\end{aligned} \tag{24}$$

$$\frac{sd(t)}{g(\mathbf{x})} \leqslant \frac{s^2}{kg^2(\mathbf{x})} + \frac{kd^2(t)}{4} \tag{25}$$

$$-\varepsilon(\mathbf{z})s \leqslant \frac{s^2}{2kg(\mathbf{x})} + \frac{kg(\mathbf{x})}{2}\varepsilon^2(\mathbf{z}) \tag{26}$$

Where, $|\varepsilon(z)| \leqslant \varepsilon^*$; $|d(t)| \leqslant d_0$; $g(\mathbf{x}) \leqslant \bar{g}$. Combining Eq. 23 further we can get:

$$\begin{aligned}\dot{V} &\leqslant -\left(\frac{1}{kg(\mathbf{x})}+\frac{1}{kg^2(\mathbf{x})}\right)s^2+\frac{s^2}{kg^2(\mathbf{x})}+\frac{kd^2(t)}{4}+\frac{s^2}{2kg(\mathbf{x})}+\frac{kg(\mathbf{x})}{2}\varepsilon^2(\mathbf{z})-\frac{\sigma}{2}\left(\|\widetilde{W}\|^2-\|W^*\|^2\right)\\ &= -\frac{s^2}{2kg(\mathbf{x})}-\frac{\sigma}{2}\|\widetilde{W}\|^2+\left(\frac{kd^2(t)}{4}+\frac{kg(\mathbf{x})}{2}\varepsilon^2(\mathbf{z})+\frac{\sigma}{2}\|W^*\|^2\right)\\ &\leqslant -\frac{s^2}{2kg(\mathbf{x})}-\frac{\sigma}{2}\|\widetilde{W}\|^2+\left(\frac{kd_0{}^2}{4}+\frac{k\bar{g}}{2}\varepsilon^{*2}(\mathbf{z})+\frac{\sigma}{2}\|W^*\|^2\right)\\ &\leqslant -\frac{1}{\alpha_0}V+\sigma_0\end{aligned} \tag{27}$$

Where:

$$\begin{aligned}\alpha_0 &= \max\left\{k,\frac{\lambda_{\max}(\Gamma^{-1})}{\sigma}\right\}\\ \sigma_0 &= \frac{kd_0{}^2}{4}+\frac{k\bar{g}}{2}\varepsilon^{*2}(\mathbf{z})+\frac{\sigma}{2}\|W^*\|^2\end{aligned} \tag{28}$$

In the formula, $\lambda_{\max}(\cdot)$ denotes the matrix maximum eigenvalue. It can be seen that when k and σ are sufficiently small, σ_0 can be arbitrarily small. Multiplying both sides of Eq. 27 by $e^{\frac{1}{\alpha_0}t}$, there have:

$$\frac{d}{dt}\left(Ve^{\frac{1}{\alpha_0}t}\right)\leqslant\sigma_0 e^{\frac{1}{\alpha_0}t} \tag{29}$$

Integrating Eq. 29 at time t yields:

$$0\leqslant V(t)\leqslant[V(0)-\sigma_0\alpha_0]\sigma_0 e^{-\frac{1}{\alpha_0}t}+\sigma_0\alpha_0 \tag{30}$$

Where, $V(0)=\frac{1}{2}\left(\frac{s^2(0)}{g(0)}+\widetilde{W}^T(0)\Gamma^{-1}\widetilde{W}(0)\right)$. According to uniform boundedness, combined with Lemma 1.1 from the literature Ge and Wang (2004), Eq. 30 can be written as:

$$0\leqslant V(t)\leqslant[V(0)-\sigma_0\alpha_0]\sigma_0 e^{-\frac{1}{\alpha_0}t}+\sigma_0\alpha_0\leqslant V(0)+\sigma_0\alpha_0 \tag{31}$$

Derived by Eq. 22:

$$\begin{aligned}&\frac{\|s(t)\|^2}{2\bar{g}}\leqslant\frac{s^2(t)}{2g(\mathbf{x})}\leqslant V(t)\\ &\frac{1}{2}\lambda_{\min}(\Gamma^{-1})\|\widetilde{W}(t)\|^2\leqslant\frac{1}{2}\widetilde{W}^T\Gamma^{-1}\widetilde{W}\leqslant V(t)\end{aligned} \tag{32}$$

Where, $\lambda_{\min}(\cdot)$ represents the matrix minimum eigenvalue. Combining Eq. 31 and Eq. 32:

$$\begin{aligned}\|s(t)\|&\leqslant\sqrt{2\bar{g}(V(0)+\sigma_0\alpha_0)}\\ \|\widetilde{W}(t)\|&\leqslant\sqrt{\frac{2V(0)+2\sigma_0\alpha_0}{\lambda_{\min}(\Gamma^{-1})}}\end{aligned} \tag{33}$$

Then the upper bounds of $\mathbf{x}$ and $\widehat{W}$ can be set as:

$$\begin{aligned}\|x_1(t)\|&\leqslant\sqrt{2\bar{g}(V(0)+\sigma_0\alpha_0)}+\|y_d(t)\|\leqslant\sqrt{2\bar{g}(V(0)+\sigma_0\alpha_0)}+\max_{\tau\in[0,t]}\{y_d(\tau)\}\\ \|x_2(t)\|&\leqslant\sqrt{2\bar{g}(V(0)+\sigma_0\alpha_0)}+\|\dot{y}_d(t)\|\leqslant\sqrt{2\bar{g}(V(0)+\sigma_0\alpha_0)}+\max_{\tau\in[0,t]}\{\dot{y}_d(\tau)\}\\ \|\widehat{W}(t)\|&\leqslant\sqrt{\frac{2V(0)+2\sigma_0\alpha_0}{\lambda_{\min}(\Gamma^{-1})}}+\|W^*\|\end{aligned} \tag{34}$$

From Eq. 30 and Eq. 32:

$$\begin{aligned}\|s(t)\|&\leqslant\sqrt{2\bar{g}\left\{[V(0)-\sigma_0\alpha_0]\sigma_0 e^{-\frac{1}{\alpha_0}t}+\sigma_0\alpha_0\right\}}\\ \|\widetilde{W}(t)\|&\leqslant\sqrt{\frac{2[V(0)-\sigma_0\alpha_0]\sigma_0 e^{-\frac{1}{\alpha_0}t}+2\sigma_0\alpha_0}{\lambda_{\min}(\Gamma^{-1})}}\end{aligned} \tag{35}$$

When time t approaches infinity:

$$\begin{aligned}&\lim_{t\to\infty}\|s(t)\|\leqslant\sqrt{2\bar{g}\sigma_0\alpha_0}\\ &\lim_{t\to\infty}\|\widetilde{W}(t)\|\leqslant\sqrt{\frac{2\sigma_0\alpha_0}{\lambda_{\min}(\Gamma^{-1})}}\end{aligned} \tag{36}$$

Therefore, for the system shown in Eq. 6, using the control rate of Eq. 17 and the weight update rate of Eq. 18, we can derive:

For any given initial compact set Ω_0:

$$\Omega_0=\left\{\mathbf{x}(0),X_d(0),\widehat{W}(0)|\mathbf{x}(0)\in\Omega_{\mathbf{x}},\widehat{W}(0)\in\Omega_{\widehat{W}},X_d(0)\in\Omega_{X_d}\right\} \tag{37}$$

There have:

(1) The neural network weight estimate $\widehat{W}(t)$ and the system state variable $\mathbf{x}(t)$ remain in the compact set Ω_1,

$$\begin{aligned}\Omega_1=\{&\mathbf{x}(t),\widehat{W}(t)\\ &\|x_1(t)\|\leqslant\sqrt{2\bar{g}(V(0)+\sigma_0\alpha_0)}+\max_{\tau\in[0,t]}\{y_d(\tau)\},\\ &\|x_2(t)\|\leqslant\sqrt{2\bar{g}(V(0)+\sigma_0\alpha_0)}+\max_{\tau\in[0,t]}\{\dot{y}_d(\tau)\},\\ &\|\widehat{W}(t)\|\leqslant\sqrt{\frac{2V(0)+2\sigma_0\alpha_0}{\lambda_{\min}(\Gamma^{-1})}}+\|W^*\|,X_d(t)\in\Omega_{X_d}\}\end{aligned} \tag{38}$$

(2) As time t approaches infinity, the sliding mode function and the neural network weight deviation values converge to the tight set Ω_n:

$$\Omega_n=\left\{s(t),\widetilde{W}(t)\left|\lim_{t\to\infty}\|s(t)\|\leqslant\sqrt{2\bar{g}\sigma_0\alpha_0},\lim_{t\to\infty}\|\widetilde{W}(t)\|\leqslant\sqrt{\frac{2\sigma_0\alpha_0}{\lambda_{\min}(\Gamma^{-1})}}\right.\right\} \tag{39}$$

Ω_0, Ω_1, Ω_n represent the initial condition compact set, response process compact set and steady state compact set, respectively. The greater the initial state deviation $e(0)$ and the neural network weight deviation $\widetilde{W}(0)$, the greater the bounds of the transient response process of the system, and Ω_0 will affect the convergence boundaries of the state and weight of Ω_1. The range of Ω_n depends on the design parameters σ_0, Γ and k, the weight deviations of the network, and the external pertur-

bations. Therefore, by choosing appropriate design parameters, the controller can have better tracking performance.

From Eq. 31, for any initial value corresponding to the tight set Ω_0, the state variables $\mathbf{x}(t)$ as well as the estimates of network weights $\widehat{W}(t)$ remain in the compact set Ω_1. Therefore, as long as the NN is large enough to cover the compact set Ω_1, ANNSMC can be ensured to be stable. The boundedness of the initial conditions ensures that the closed-loop signal remains bounded during the response process.

CRediT authorship contribution statement

Yiqi Liu: Conceptualization, Data curation, Formal analysis, Funding acquisition, Writing – original draft. **Jing Zhang:** Conceptualization, Data curation, Formal analysis, Writing – review & editing. **Zhuyi Qiu:** Conceptualization, Data curation, Visualization, Writing – review & editing. **Yigang Zhang:** Conceptualization, Data curation, Formal analysis. **Guangping Yu:** Conceptualization, Data curation, Formal analysis. **Hongtao Ye:** Supervision, Data curation, Resources. **Zefan Cai:** Project administration, Writing – review & editing.

Declaration of competing interest

All authors disclosed no relevant relationships.

Data availability

Data will be made available on request

Acknowledgements

This work was supported by the National Natural Science Foundation of China (Grant No.: 62273151, 62073145), the Guangdong Basic and Applied Basic Research Foundation (Grant No.: 2021B1515420003), the Guangdong Generic Institution Innovation Team Research Foundation (Grant No.: 2023KCXTDO72).

Supplementary material

Supplementary material associated with this article can be found, in the online version, at 10.1016/j.wroa.2024.100245

References

Baeten, J.E., Batstone, D.J., Schraa, O.J., van Loosdrecht, M.C., Volcke, E.I., 2019. Modelling anaerobic, aerobic and partial nitritation-anammox granular sludge reactors-a review. Water Res. 149, 322–341.
Boiocchi, R., Gernaey, K.V., Sin, G., 2016. Systematic design of membership functions for fuzzy-logic control: a case study on one-stage partial nitritation/anammox treatment systems. Water Res. 102, 346–361.
Boruah, N., Roy, B., 2019. Event triggered nonlinear model predictive control for a wastewater treatment plant. J. Water Process Eng. 32, 100887.
Cao, W., Yang, Q., 2020. Online sequential extreme learning machine based adaptive control for wastewater treatment plant. Neurocomputing 408, 169–175.
Chen, K., Wang, H., Valverde-Pérez, B., Zhai, S., Vezzaro, L., Wang, A., 2021. Optimal control towards sustainable wastewater treatment plants based on multi-agent reinforcement learning. Chemosphere 279, 130498.
Cheng, H., Wu, J., Huang, D., Liu, Y., Wang, Q., 2021. Robust adaptive boosted canonical correlation analysis for quality-relevant process monitoring of wastewater treatment. ISA Trans. 117, 210–220.
Ching, P.M., So, R.H., Morck, T., 2021. Advances in soft sensors for wastewater treatment plants: a systematic review. J. Water Process Eng. 44, 102367.
DeVore, R., Hanin, B., Petrova, G., 2021. Neural network approximation. Acta Numerica 30, 327–444.
Du, S., Zhang, Q., Han, H., Sun, H., Qiao, J., 2022. Event-triggered model predictive control of wastewater treatment plants. J. Water Process Eng. 47, 102765.
Fujio, T., Shibasaki, H., Tanaka, R., Murakami, T., Ishida, Y., 2016. Sliding mode control based on a modified linear control input. Int. J. Control Automat. Syst. 14, 115–127.
Ge, S.S., Wang, C., 2004. Adaptive neural control of uncertain mimo nonlinear systems. IEEE Trans. Neural Netw. 15 (3), 674–692.
Han, H., Liu, H., Li, J., Qiao, J., 2020. Cooperative fuzzy-neural control for wastewater treatment process. IEEE Trans. Ind. Inf. 17 (9), 5971–5981.
Han, H., Liu, Z., Li, J., Qiao, J., 2021. Design of syncretic fuzzy-neural control for wwtp. IEEE Trans. Fuzzy Syst. 30 (8), 2837–2849.
Han, H., Wu, X., Qiao, J., 2018. A self-organizing sliding-mode controller for wastewater treatment processes. IEEE Trans. Control Syst. Technol. 27 (4), 1480–1491.
Harja, G., Nascu, I., Muresan, C., Nascu, I., 2016. Improvements in dissolved oxygen control of an activated sludge wastewater treatment process. Circuit. Syst. Signal Process. 35, 2259–2281.
Iratni, A., Chang, N.-B., 2019. Advances in control technologies for wastewater treatment processes: status, challenges, and perspectives. IEEE/CAA J. Automatica Sinica 6 (2), 337–363.
Jeppsson, U., Pons, M.-N., Nopens, I., Alex, J., Copp, J., Gernaey, K., Rosen, C., Steyer, J.-P., Vanrolleghem, P., 2007. Benchmark simulation model no 2: general protocol and exploratory case studies. Water Sci. Technol. 56 (8), 67–78.
Li, D., Yang, C., Li, Y., 2024. A multi-subsystem collaborative bi-lstm-based adaptive soft sensor for global prediction of ammonia-nitrogen concentration in wastewater treatment processes. Water Res. 121347.
Li, D., Zou, M., Jiang, L., 2022. Dissolved oxygen control strategies for water treatment: a review. Water Sci. Technol. 86 (6), 1444–1466.
Liu, Y., Yuan, J., Cai, B., Chen, H., Li, Y., Huang, D., 2023. Multi-step and multi-task learning to predict quality-related variables in wastewater treatment processes. Process Saf. Environ. Protect. 180, 404–416.
Liu, Y., Yuan, L., Huang, S., Huang, D., Liu, B., 2020. Integrated design of monitoring, analysis and maintenance for filamentous sludge bulking in wastewater treatment. Measurement 155, 107548.
Monteiro, M.T.T., Santo, I.E., Rodrigues, H.S., 2022. An optimal control problem applied to a wastewater treatment plant. Discrete Contin. Dyn. Syst.-Ser. S 15 (3).
Munoz, C., Young, H., Antileo, C., Bornhardt, C., 2009. Sliding mode control of dissolved oxygen in an integrated nitrogen removal process in a sequencing batch reactor (sbr). Water Sci. Technol. 60 (10), 2545–2553.
Piotrowski, R., Sawicki, H., Żuk, K., 2021. Novel hierarchical nonlinear control algorithm to improve dissolved oxygen control in biological wwtp. J. Process Control 105, 78–87.
Pozevalkin, V., Parfenov, I., Polyakov, A., 2019. Approximation of machine tool experimental thermal characteristics by neural network. Journal of Physics: Conference Series, Vol. 1399. IOP Publishing, p. 044018.
Riaz, S., Yin, C.-W., Qi, R., Li, B., Ali, S., Shehzad, K., 2023. Design of predefined time convergent sliding mode control for a nonlinear pmlm position system. Electronics 12 (4), 813.
Tzoneva, R., 2007. Optimal pid control of the dissolved oxygen concentration in the wastewater treatment plant. AFRICON 2007. IEEE, pp. 1–7.
Vilanova, R., Alfaro, V., et al., 2009. Multi-loop pi-based control strategies for the activated sludge process. 2009 IEEE Conference on Emerging Technologies & Factory Automation. IEEE, pp. 1–8.
Wahab, N.A., Katebi, M., Balderud, J., 2007. Multivariable pid control design for wastewater systems. 2007 Mediterranean Conference on Control & Automation. IEEE, pp. 1–6.
Ye, H.-t., Li, Z.-q., Luo, W.-g., 2013. Dissolved oxygen control of the activated sludge wastewater treatment process using adaptive fuzzy pid control. Proceedings of the 32nd Chinese Control Conference. IEEE, pp. 7510–7513.
Zhang, J., Yan, H., Chen, H., Xu, S., Liu, Y., 2023. Multi-objective optimal control of wastewater treatment processes constrainted by energy-saving and effluent qualities. 2023 6th International Conference on Robotics, Control and Automation Engineering (RCAE). IEEE, pp. 229–233.